THE ASTROPHYSICAL JOURNAL, 465:887–897, 1996 July 10

GALACTIC EVOLUTION OF D AND ^{3}He INCLUDING STELLAR PRODUCTION OF ^{3}He

DAVID S. P. DEARBORN,[1] GARY STEIGMAN,[2] AND MONICA TOSI[3]

Received 1995 October 10; accepted 1996 January 25

ABSTRACT

New stellar models which track the production and destruction of ^{3}He (and D) have been evolved for a range of stellar masses ($0.65 \leq M/M_\odot \leq 100$), metallicities ($0.01 \leq Z/Z_\odot \leq 1$), and initial (main-sequence) ^{3}He mass fractions ($10^{-5} \leq X_{3,\rm MS} \leq 10^{-3}$). Armed with the ^{3}He yields from these stellar models we have followed the evolution of D and ^{3}He using a variety of chemical evolution models with and without infall of primordial or processed material. Production of new ^{3}He by the lower mass stars overwhelms any reasonable primordial contributions and leads to predicted abundances in the presolar nebula and/or the present interstellar medium in excess of the observationally inferred values. This result, which obtains even for zero primordial D and ^{3}He, and was anticipated by Rood, Steigman, & Tinsley is insensitive to the choice of chemical evolution model; it is driven by the large ^{3}He yields from low-mass stars. In an attempt to ameliorate this problem we have considered a number of nonstandard models in which the yields from low-mass stars have been modified. Although several of these nonstandard models may be consistent with the ^{3}He data, they may be inconsistent with observations of ^{12}C/^{13}C, ^{18}O, and, most seriously, the super–^{3}He rich planetary nebulae. Even using the most extreme of these nonstandard models we obtain a generous upper bound to pregalactic ^{3}He: $X_{3P} \leq 3.2 \times 10^{-5}$ which, nonetheless, leads to a stringent lower bound to the universal density of nucleons.

Subject headings: nuclear reactions, nucleosynthesis, abundances — stars: interiors

1. INTRODUCTION

To test and constrain models of primordial nucleosynthesis it is necessary to confront the predicted abundances with observational data. Such comparisons are complicated by the necessity of extrapolating the abundances inferred "here and now" (solar system, interstellar medium, etc.) to their "there and then" (primordial or pregalactic) universal values. This difficulty is somewhat ameliorated for ^{4}He which is observed in less evolved, low-metallicity extragalactic H II regions (e.g., Pagel et al. 1991; Skillman et al. 1994; Olive & Steigman 1995) and for ^{7}Li which is probed in metal-poor halo stars (Spite & Spite 1982; Thorburn 1994). In contrast, ^{3}He is only observed in the solar system (Black 1971, 1972; Geiss & Reeves 1972; Geiss 1993) and in Galactic H II regions (Bania, Rood, & Wilson 1987; Balser et al. 1994). Until recently, D too had only been observed "here and now." A new era in probing deuterium has dawned with the identification of possible absorption of QSO light by high-redshift D (Carswell et al. 1994; Songaila et al. 1994; Tytler 1995). However, "wrong velocity" hydrogen absorbers may masquerade as deuterium (Carswell et al. 1994; Songaila et al. 1994; Steigman 1994) so that much more data are required before such observations may be used to fix the nearly primordial abundance of D. Thus, to infer the pregalactic abundances of D and ^{3}He it is currently necessary to have recourse to models of galactic chemical evolution. Unfortunately, the uncertainties and/or lack of uniqueness of such models compound the observational uncertainties.

The evolution of D is straightforward since, when incorporated in a star it is burned (to ^{3}He) during the pre–main-sequence evolution. If the "virgin" fraction of the interstellar medium (ISM; either today or at the time of formation of the solar system 4.5 Gyr ago) were known, the primordial D abundance could be inferred from ISM or solar system observations. A very large class of chemical evolution models (Audouze & Tinsley 1974; Tosi 1988a, b; Vangioni-Flam & Audouze 1988; Matteucci & François 1989; Steigman & Tosi 1992), constrained by heavy element abundances, abundance gradients, abundance ratios (primary vs. secondary), and cosmochronometers, find that $\sim\frac{1}{3}$–$\frac{2}{3}$ of the ISM (now, t_0 or, at the time of the solar system formation, $t_\odot$) has never been through stars. However, "designer models" with larger D destruction (Vangioni-Flam, Olive, & Prantzos 1994; Olive et al. 1995; Scully & Olive 1995) do exist, but see, e.g., Edmunds (1994) and Prantzos (1995) for their consistency problems.

The galactic evolution of ^{3}He is complex. Any prestellar ^{3}He is enhanced by the pre–main-sequence burning of prestellar D. Thus, when a star reaches the main sequence, the ^{3}He mass fraction exceeds that in the prestellar nebula [$X_{3,\rm MS} = (X_3 + 3X_2/2)_{\rm pre}$; in what follows we write X_i for mass fractions and y_i for ratios by number to hydrogen; $y_{ij} \equiv y_i + y_j$]. ^{3}He survives nuclear burning in the cooler outer layers of stars, is destroyed in the hotter interiors and, especially in low-mass stars, is synthesized via hydrogen burning. Thus, depending on the mass (and, to a lesser extent the metallicity) of a star, ^{3}He is preserved, produced, or destroyed. To understand the galactic evolution of ^{3}He, it is necessary to first understand its stellar evolution (Iben 1967; Rood 1972; Dearborn, Schramm, & Steigman 1986; Vassiliadis & Wood 1993). However, since *some* ^{3}He survives stellar processing and, prestellar D is burned to ^{3}He, the evolution of ^{3}He (or, D + ^{3}He) is less rapid than that of D alone (Yang et al. 1984, hereafter YTSSO). Thus, observations of D and ^{3}He (e.g., in the solar system) may be used to infer an *upper bound* to primordial D and/or D + ^{3}He (YTSSO; Walker et al. 1991, hereafter WSSOK). As a result, models which destroy D more efficiently are to some

[1] Lawrence Livermore National Laboratory L-58, P.O. Box 808, Livermore, CA 94550.
[2] Departments of Physics and Astronomy, The Ohio State University, 174 West 18th Avenue, Columbus, OH 43210.
[3] Osservatorio Astronomico di Bologna, Via Zamboni 33, 40126 Bologna, Italy.

extent constrained by the requirement that solar system and/or ISM ^{3}He not be overproduced.

Rood, Steigman, & Tinsley (1976, hereafter RST) first included stellar production of ^{3}He in numerical models of galactic evolution. RST found that stellar production led to a rapid increase in X_3 from $t_\odot$ to t_0 which seemed in conflict with the then current observations (bounds only) and concluded that it seemed unlikely that ^{3}He could be used cosmologically. As we shall see, this problem persists today (Olive et al. 1995).

In a previous study (Steigman & Tosi 1992, hereafter ST92) we used the ^{3}He survival from Dearborn, Schramm, & Steigman (1986) in models of galactic evolution consistent with a large number of observational constraints (Tosi, 1988a) to track the evolution of D and ^{3}He. Not including ^{3}He production in low mass stars, we found that $X_{3P} \approx X_{3\odot} \approx X_{30}$ for a wide range of choices of initial (primordial) abundances for D and ^{3}He. Similar results have been found, e.g., by Fields (1995). At the same time, the ^{3}He H II region data (Bania et al. 1987; Rood, Bania, & Wilson 1992) have been supplemented by new and important observations of super–^{3}He-rich material in a few planetary nebulae (Balser et al. 1994; Rood et al. 1995, hereafter RBWB95). Since the gas in planetary nebulae (PNs) reflects the chemical composition of the ejected outer layers of their central stars, where the original ^{3}He abundance has certainly been modified by stellar processing, their large ^{3}He abundances should not be taken as representative of the ISM abundances at the time of the formation of their central stars, but rather as the result of stellar nucleosynthesis in low-mass stars. The observed abundances lend support to the estimates of newly synthesized ^{3}He ($X_{3*} \approx 0.7$–7×10^{-3}) in low-mass stars (0.6–2.3 $M_\odot$) in the pioneering work of Iben (1967) and Rood (1972), and makes timely a reinvestigation of the galactic evolution of ^{3}He (along with D) *including* stellar production of ^{3}He (Galli et al. 1995: Tosi, Steigman, & Dearborn 1995; Olive et al. 1995). To this aim, we have computed an extensive grid of stellar evolution models with varying initial abundances of ^{3}He and of the overall metallicity Z, and we have reexamined the galactic evolution of D and ^{3}He in the framework of such stellar models.

In § 2 we describe the stellar models we have evolved to follow the evolution of ^{3}He and present our results for the survival/production of ^{3}He as a function of stellar mass ($0.65 \leq M/M_\odot \leq 100$), metallicity ($Z = 0.02$, 0.002, 0.0002), and initial (main sequence $\Rightarrow$ D + ^{3}He) ^{3}He ($10^5 X_{3,\mathrm{MS}} =$ 1.0, 5.0, 10, 21, 100). In § 3 and § 4 we use the stellar results in a series of chemical evolution models (Tosi 1988a, b; ST92) to follow the galactic evolution of D and ^{3}He. In § 5 we further follow the ^{3}He evolution modifying the stellar yields. Sections 6 and 7 are reserved for discussions and conclusions.

2. STELLAR EVOLUTION OF ^{3}He

The evolution of stars with $M = 0.65$–$100\ M_\odot$ and three metallicities (Population I: $X = 0.70$, $Z = 0.02$; Population I$\frac{1}{2}$: $X = 0.76$, $Z = 0.002$; Population II: $X = 0.76$, $Z = 0.0002$) was followed using the code described in Dearborn, Griest, & Raffelt (1991) which is derived from that of Eggleton (1967, 1968). OPAL opacities (Iglesias & Rogers 1990, 1992) are used for temperatures above 6000 K and Los Almos opacities (Heubner et al. 1977), including the contribution of molecules, for lower temperatures. Our code follows ^{3}He production and destruction in all hydrogen-burning regions and a postprocessor is used to calculate the nucleosynthesis of D and the isotopes of Li, Be, C, N, O, and several other elements. Calculations with this postprocessor confirmed the pre–main-sequence conversion of D to ^{3}He. The mixing length is chosen to give the correct solar radius; this model predicts a neutrino flux (for the chlorine experiment) of 7.9 SNU and the p-mode spectrum matches that of Bahcall & Ulrich (1988). For the Population I$\frac{1}{2}$ and Population II models, a slightly larger mixing length is required to fit the color-magnitude data of M30 (Bolte 1994). However, ^{3}He evolution is insensitive to any reasonable choice of mixing length.

All models began in the pre–main sequence on the Hayashi track. The final evolutionary state depended on the mass of the star. Stars with $0.65 \leq M/M_\odot \leq 2.00$ were evolved up to the helium flash. For one model (1.5 $M_\odot$) the evolution was followed through the helium flash and up the asymptotic giant branch (AGB). This additional evolution (without thermal pulses) changed the ^{3}He mass fraction in the envelope by less than 1%, demonstrating that in the absence of thermal pulses, the envelope abundance of ^{3}He is insensitive to the subsequent (post helium flash) evolution of these stars. Intermediate-mass stars ($2.5 \leq M/M_\odot \leq 8.0$) were all evolved to the AGB, to a point where mass loss (and possible planetary nebula formation) dominates their remaining evolution. All massive-star models ($M \geq 10\ M_\odot$) were evolved into carbon burning stages and are within a few thousand years of core collapse, leaving insufficient time for significant changes in the composition of their hydrogen envelopes. We have not allowed for winds and this suggests that, for the more massive stars, we have underestimated the ^{3}He returned to the ISM (see, e.g., Dearborn, Schramm, & Steigman 1986).

Since D is completely burned to ^{3}He in the pre–main sequence, our main sequence (MS) ^{3}He abundance reflects the prestellar contribution from D and ^{3}He: $X_{3,\mathrm{MS}} = X_3 + 3X_2/2$. To explore the sensitivity of our ^{3}He yields [envelope fractions X_3(env)] to $X_{3,\mathrm{MS}}$ we have chosen five values of $X_{3,\mathrm{MS}}$ from 1×10^{-5} to 1×10^{-3}. The top panel of Figure 1 shows our Population I yields $X_{3f} \equiv X_3$(env) as a function of the initial stellar mass for different choices of $X_{3,\mathrm{MS}}$. For lower mass stars production dominates and, when convection on the giant branch homogenizes the envelope, the ^{3}He available to be returned to the ISM is strongly enhanced. Without substantial mass loss, these lower mass stars remain near the Hayashi track during helium burning and beyond. In the absence of a hot bottom convection zone stimulated by thermal pulses, there is no destruction of this "new" ^{3}He. For more massive stars the lifetimes are shorter resulting in less ^{3}He production in the temperature regimes where this occurs. Note that if these stars started with no initial ^{3}He they would, in fact, be net producers of ^{3}He; in this case $g_3 \equiv X_{3f}/X_{3,\mathrm{MS}}$ would diverge. However, for the range of $X_{3,\mathrm{MS}}$ of interest (10^{-5}–10^{-3}), the small production of ^{3}He in more massive stars does not compensate for the destruction of initial ^{3}He.

A striking feature of the 15 and 25 $M_\odot$ Population I models is the dip in X_{3f}. The high envelope opacity allowed these models to homogenize the envelope on the giant branch prior to helium burning. The blue loop that occurred during helium burning then led to a second epoch of ^{3}He destruction. In contrast, the 50 and 100 $M_\odot$ models completed their helium burning before evolving to the red,

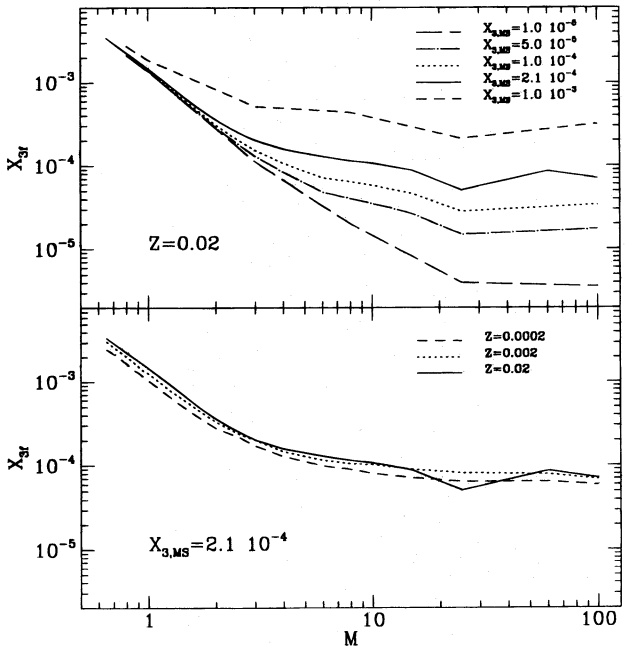

FIG. 1.—*Top panel:* final envelope abundance of ^{3}He as a function of the stellar initial mass for five different main-sequence abundances of ^{3}He and $Z = 0.02$. *Bottom panel:* final envelope abundance of ^{3}He as a function of the stellar initial mass for three different metallicities and $X_{3,MS} = 2.1 \times 10^{-4}$.

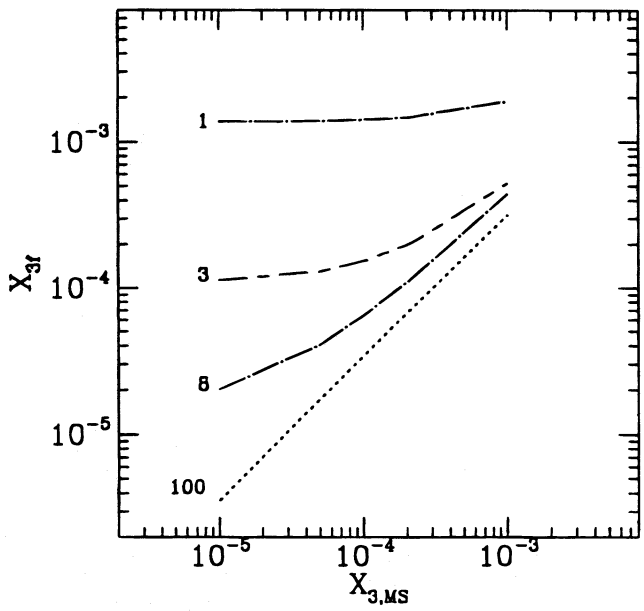

FIG. 2.—Final envelope abundance of ^{3}He for $Z = 0.02$ in stars of initial mass $M/M_\odot = 1$, 3, 8, and 100 as a function of the main-sequence abundance.

thus leading to the "recovery" of X_{3f} seen in the top panel of Figure 1. Similarly, the lower metallicity ($Z = 0.002$ and $Z = 0.0002$) 25 $M_\odot$ models did not evolve all the way to the red giant branch prior to helium burning and, therefore, these stars only experienced ^{3}He destruction on the main sequence (see bottom panel of Fig. 1). For Population I$\frac{1}{2}$ and Population II stars the lower opacity results in a more compact, warmer structure (similar to that of a slightly more massive Population I star). At a fixed mass this leads to a shorter lifetime resulting in less production and more destruction of ^{3}He. However, the lower metallicity 15 and 25 $M_\odot$ models do not experience a second epoch of ^{3}He destruction. As a result, they show less ^{3}He destruction than the Population I models (i.e., no dip in X_{3f} vs. $X_{3,MS}$). By comparing the two panels of Figure 1, it is apparent that the amount of ^{3}He ejected by stars depends much more on its main-sequence ^{3}He abundance than on the overall stellar metallicity.

In Figure 2 we display our $Z = 0.02$ (Population I) results from a different perspective by showing the final yield (X_{3f}) as a function of the initial abundance ($X_{3,MS}$) for $1 \leq M/M_\odot \leq 100$. For $M = 1\ M_\odot$, production dominates and X_{3f} is (nearly) independent of $X_{3,MS}$ (except at the highest $X_{3,MS}$). In contrast, for $M = 100\ M_\odot$ production is negligible and X_{3f} varies linearly with $X_{3,MS}$. The transition from low- to high-mass models is seen for $M = 3$ and $8\ M_\odot$. For $0.65 \leq M/M_\odot \leq 2.5$, where production dominates, we find $X_{3f} \approx (M_\odot/M)^{2.2} \times 10^{-3}$. For more massive stars the relation between X_{3f} and $X_{3,MS}$ is more complex. As $X_{3,MS}$ increases, ^{3}He production is relatively less important, resulting in the curvature seen in Figure 2 for $M = 3$ and $8\ M_\odot$. For high masses where production is negligible, $X_{3f} \approx 0.33 X_{3,MS}$.

In the absence of ^{3}He production it is interesting to consider the ^{3}He "survivial fraction" $g_3 \equiv X_{3f}/X_{3,MS}$ (Dearborn, Schramm, & Steigman 1986; YTSSO; ST92). In the presence of ^{3}He production g_3 is less useful and potentially misleading since the yield is not proportional to $X_{3,MS}$. Nonetheless, for comparison with previously published results, g_3 versus M for our five choices of $X_{3,MS}$ is shown in Figure 3. The divergence of the curves at low M reflects the increasing importance of ^{3}He production which sets in first (at the largest M) for the lowest values of $X_{3,MS}$. Note that in the limit that $X_{3,MS}$ goes to zero, g_3 diverges. In Figure 4 is shown $\langle g_3 \rangle$, the value of g_3 averaged over Tinsley's (1980) IMF as a function of the lower mass limit m_l of the IMF. For gas incorporated in a generation of stars, as time increases material is returned from lower mass stars and so Figure 4 provides a picture of the time evolution of the ^{3}He "suvival." Note that for all m_l, $\langle g_3 \rangle \gtrsim 0.3$. Depending on the initial abundance, production dominates, $\langle g_3 \rangle \gtrsim 1$, for m_l up to $7\ M_\odot$. In terms of galactic evolution this implies that the ISM starts to be enriched in ^{3}He as soon as stars less massive than 3–7 $M_\odot$ (depending on the initial ^{3}He abundance) start to die. We note again that stars

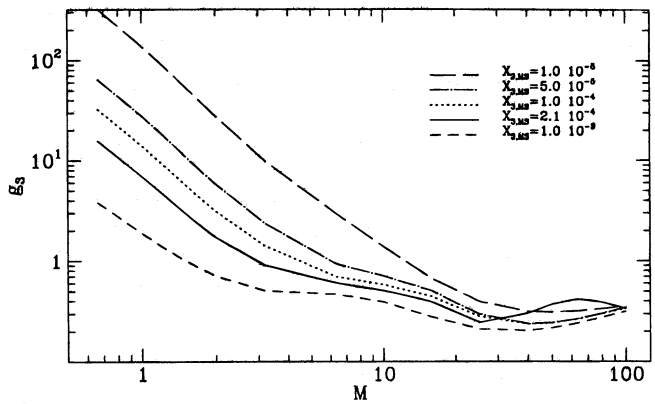

FIG. 3.—Survival fraction g_3 of ^{3}He as a function of the stellar initial mass for $Z = 0.02$ and five different main-sequence abundances of ^{3}He.

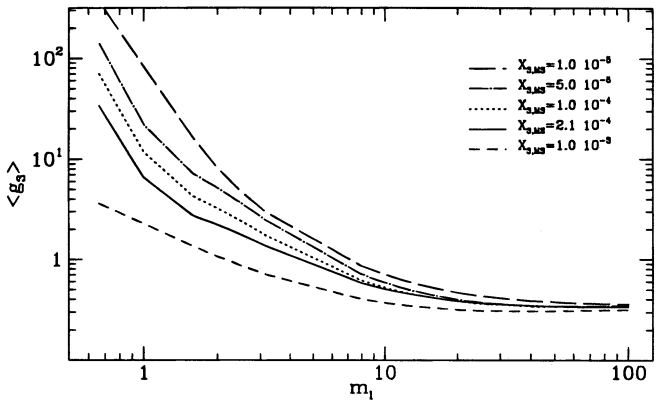

FIG. 4.—Average g_3 convolved with Tinsley's (1980) IMF as a function of the lower mass limit m_l on the IMF integral.

above $\sim 25\ M_\odot$ are likely to experience mass loss which will return unburnt ^{3}He to the ISM. For massive stars our neglect of mass loss results in an underestimate of g_3.

The trends in our results are easy to understand. During the hydrogen-burning phase ^{3}He is produced in the core of stars of all masses. However, with time, the core temperature (which depends on stellar mass) increases to values where ^{3}He is burned. Thus, new ^{3}He survives only in a radiative shell adjacent to the convective core and, from this shell, may later be dredged up to the surface where it will mix with the prestellar main-sequence ^{3}He. The competition between net production or destruction then depends not only on $X_{3,\mathrm{MS}}$ but on the size of the shell and the amount of new ^{3}He there, and on the depth of the dredge-ups (i.e., whether they bring to the surface material which is enhanced or depleted in ^{3}He). In low mass stars much new ^{3}He is produced and most of it survives to dominate over (reasonably small values of) $X_{3,\mathrm{MS}}$. In contrast, for massive stars little new ^{3}He is synthesized in the core, destruction is efficient and the ^{3}He preservation shell is small so that the intial ^{3}He dominates.

We note that the Eggleton-type code we use permits larger time steps on the AGB which tends to suppress thermal pulses. However, when short time steps are enforced, these pulses occur. Such pulses are plausible sites for the lithium enhancements, produced at the expense of ^{3}He, observed in some S-type stars. Although it does not require much ^{3}He depletion to yield huge lithium enhancements, since the lithium is fragile it is possible that the lithium enhancement attains a steady state with ^{3}He processed to ^{4}He. A limit on such ^{3}He processing might follow from the fact that a very fragile nucleus, ^{18}O, survives the dredge-up in normal carbon stars (Dearborn 1992). Since ^{3}He is destroyed at higher temperatures than those for ^{18}O, the lack of ^{18}O depletion suggests that ^{3}He is not strongly depleted in normal carbon stars.

A similar argument applies to the main-sequence mixing proposed to explain the low ^{12}C/^{13}C ratios observed in red giants (Dearborn & Eggleton 1976; Dearborn 1992). In red giants ^{18}O appears to be independent of the ^{13}C enhancement, perhaps due to stabilization by a molecular weight gradient. Since it is difficult to mix with a region of depleted ^{3}He without modifying ^{18}O, it is suggestive that ^{3}He is not destroyed in these stars. In contrast, J-type carbon stars have CNO-equilibrium vaues for ^{12}C/^{13}C and do show ^{18}O depletions. In such stars ^{3}He is likely destroyed throughout the envelope. If most carbon stars pass through such a stage (rather than these representing a separate class of stars), little ^{3}He may survive. Pinsonneault (1995, private communication) has noted that for solar-metalicity stars, the open cluster M67 seems to be the dividing line between stars which do not undergo giant-branch mixing and those which do, suggesting that mixing for stars with $M \gtrsim 1.3$–$1.5\ M_\odot$ is inconsistent with the ^{12}C/^{13}C data.

It is interesting to compare our results with the recent work of Vassiliadis & Wood (1993). We both agree that in the low-mass stars there is no significant change in ^{3}He between the first and second dredge-up. Further, Vassiliadis & Wood calculate thermal pulses and, for stars less than 5 $M_\odot$, they find no change in the ^{3}He abundance. Our mixing-length approximations are nearly the same even though they included a wind which stripped the envelope on the AGB while we did not. Quantitatively, our yields and theirs are in excellent agreement [provided that their $\theta(^3\mathrm{He})$ is a mass fraction] despite the fact that their opacities are different (higher) than ours and they used slightly older nuclear reaction rates.

3. THE GALACTIC EVOLUTION OF D

As in ST92 we have followed the evolution of D and ^{3}He for the two "best" chemical evolution models for the galactic disk identified in Tosi (1988a) along with a third model in which, for comparison, infall is absent. Model 1, the "best" model (Tosi 1988a; Giovagnoli & Tosi, 1995), consistent with the major observational constraints, has an exponentially decreasing SFR (with a 15 Gyr e-folding time), depending on both the gas and total mass density currently observed in each ring, a constant (in time), uniform (in space) infall rate of 0.004 $M_\odot$ kpc^{-2} yr^{-1} and uses Tinsley's (1980) initial mass function (IMF). Model 25, the "second best" model (Tosi 1988a) also has an exponentially decreasing star formation rate (SFR) with, however, a 5 Gyr e-folding time, an effectively constant (e-folding time of 100 Gyr) infall rate of uniform density 0.002 $M_\odot$ kpc^{-2} yr^{-1} and Tinsley's (1980) IMF. Our comparison no-infall models uses the same IMF and SFR e-folding time as model 1 but is normalized so as to reproduce the current SFR and gas/total mass distributions with galactocentric distance. We recall, however, that such a model does not reproduce the major features (distribution with time and galoctocentric distance of the chemical abundances) observed in the galactic disk.

Normally, our models adopt 13 Gyr for the present epoch and 8.5 Gyr for the formation of the solar system. To explore the sensitivity to the age of the model, we have run some models (indicated by a subscript 10) where the present epoch is 10 Gyr and solar system formation is at 5.5 Gyr.

Since infall plays an important role in models 1 and 25, it is necessary to specify the chemical composition of the infalling gas. We have considered models with primordial infall ($Z_{\mathrm{inf}} = 0$) for which $X_{2\mathrm{inf}} = X_{2P}$ and $X_{3\mathrm{inf}} = X_{3P}$ as well as models with partially processed infalling material. In the latter cases we have adopted $Z_{\mathrm{inf}} = 0.2\ Z_\odot$, a value low enough to preserve the infall dilution efficiency and keep the model predictions in agreement with the observational constraints in the solar neighborhood and in the whole disk (Tosi 1988b; Matteucci & François 1989). When $Z_{\mathrm{inf}} = 0.2\ Z_\odot$, the infall abundance of D is certainly lower than primordial due to stellar processing, whereas the ^{3}He abundance in principle can be either lower or higher depending

on the mass of the stars contributing to the enrichment of the accreted gas. We have thus considered models with $X_{2inf} = 0.7X_{2P}$ or $X_{2inf} = 0.8X_{2P}$ and $X_{3inf} = 0.8X_{3P}$ or $X_{3inf} = 1.2X_{3P}$. From a series of model checks we find that larger deviations of the infall abundances of D from the primordial value would be rather improbable with an overall metallicity $Z_{inf} = 0.2\,Z_\odot$.

To explore the sensitivity of our results to the primordial values we have run each model for a range of choices of X_{2P} and X_{3P} ($0 \le 10^5 X_{2P} \le 9.0$; $0 \le 10^5 X_{3P} \le 4.0$). In Table 1 we list the set of models explored.

The evolution of deuterium is straightforward since any D incorporated in stars is destroyed. Thus, the D survival factor, $f_2 = X_2/X_{2P}$, is identical to the fraction of the ISM that has never been through stars. Then f_2, is independent of X_{2P} and purely reflects the chemical evolution model. In Figure 5 we show f_2 evaluated at the solar ring ($R = 8$ kpc) as a function of time. For each model (1 and 25) we show the differences between primordial infall ($Z_{inf} = 0$, $X_{2inf} = X_{2P}$) and nonprimordial infall $Z_{inf} = 0.2\,Z_\odot$, $X_{2P} = 0.8X_{2P}$) as well as the corresponding no-infall (NI) model. We also compare in Figure 5 models whose present age is 13 Gyr with 10 Gyr models. The models with nonprimordial infall have less D refueling of the ISM and show a steeper decrease with time of f_2 than models with primordial infall. The NI model destroys D more slowly at first but, without replenishment of ISM D via infall, eventually has the largest D depletion. The short lifetime models (10 Gyr) have less time to destroy D but, to reproduce present observations have higher initial mass and SFR than the 13 Gyr models. The net result of this balancing act is that the 10 Gyr (infall) models have higher $f_{2\odot}$ but lower f_{20}; the NI models have

TABLE 1

MODELS WITH ^{3}He EVOLUTION AND INFALL

Model[a]	10^5X_{2P}	10^5X_{3P}	Model[a]	10^5X_{2P}	10^5X_{3P}
Models with Standard ^{3}He Evolution and Primordial Infall					
1-M-Ia.....	0.0	0.0	1-K-Ia	4.0	1.0
1-A-Ia	2.5	2.0	1-O-Ia	4.5	0.0
1-H-Ia	3.0	0.0	1-C-Ia	5.0	2.0
1-I-Ia	3.0	2.0	1-X-Ia	6.0	0.0
1-B-Ia.....	3.0	2.5	1-W-Ia	6.0	2.0
1-J-Ia	3.0	4.0	1-R-Ia	6.0	4.0
1-L-Ia.....	3.85	0.0	1_{10}-B-Ia	3.0	2.5
Models with Standard ^{3}He Evolution and Nonprimordial Infall					
1-K-Ib	4.0	1.0	1-W-Ib	6.0	2.0
1-K-Ic	4.0	1.0	1-W-Ic	6.0	2.0
1-K-Id	4.0	1.0	1-W-Id	6.0	2.0
1-C-Ib	5.0	2.0	1-W-Ie	6.0	2.0
Models with Nonstandard ^{3}He Evolution and Primordial Infall					
1-T-IIIa.....	6.0	1.5	25-T-IIIa	6.0	1.5
1_{10}-T-IIIa	6.0	1.5	25_{10}-T-IIIa	6.0	1.5
Models with Nonstandard ^{3}He Evolution and Nonprimordial Infall					
1-H-VIIIb	3.0	0.0	1-Q-IIIb	6.0	3.0
1-K-Vd	4.0	1.0	1-Q-Vb	6.0	3.0
1-K-VIIIb	4.0	1.0	1-U-VIb	6.0	3.5
1-V-Vb	5.0	0.0	1-R-VIb	6.0	4.0
1-S-Vb	5.0	1.0	1_{10}-H-VIIIb	3.0	0.0
1-C-IIb	5.0	2.0	1_{10}-C-VIb	5.0	2.0
1-C-IIIb	5.0	2.0	1_{10}-T-IIIb	6.0	1.5
1-C-IVb	5.0	2.0	1_{10}-W-VIIIb	6.0	2.0
1-C-Vb	5.0	2.0	25-H-VIIIb	3.0	0.0
1-C-VIb	5.0	2.0	25-K-VIIIb	4.0	1.0
1-C-VII	5.0	2.0	25-C-VIb	5.0	2.0
1-C-VIIIb	5.0	2.0	25-C-VIIIb	5.0	2.0
1-T-IIIb	6.0	1.5	25-T-IIIb	6.0	1.5
1-T-Vb.....	6.0	1.5	25_{10}-H-VIIIb	3.0	0.0
1-W-IIb.....	6.0	2.0	25_{10}-T-IIIb	6.0	1.5
1-W-IIIb.....	6.0	2.0	NI-C-III	5.0	2.0
1-W-Vb.....	6.0	2.0	NI-Z-III	9.0	1.5
1-W-VIb.....	6.0	2.0	NI_{10}-C-III	5.0	2.0
1-W-VIIIb.....	6.0	2.0	NI_{10}-Z-III	9.0	1.5

[a] Arabic numbers refer to the type of chemical evolution model (see text and Tosi 1988a). Capital letters indicate the adopted primordial abundances. Roman numerals indicate the stellar yields adopted for ^{3}He: I, as described in § 2; II, as for model I but with $g_3 = 1$ for $M < 2M_\odot$; III, as for model I but with $g_3 = 1$ for stars with $1 < M/M_\odot < 2$; IV, as for model I but with total ^{3}He destruction in stars with $M \le 1M_\odot$; V, following Pinsonneault (1995); VI, following Hogan (1995); VII, as for model VI but with ^{3}He destruction for $M \le 1.6\,M_\odot$; VIII, as for model VI but with ^{3}He destruction in the range $1.3 < M/M_\odot < 2.5$. Lower case letters indicate the adopted infall abundances: a, $X_{2inf} = X_{2p}$ and $X_{3inf} = X_{3p}$; b, $X_{2inf} = 0.8X_{2p}$ and $X_{3inf} = X_{3p}$; C, $X_{2inf} = 0.8X_{2p}$ and $X_{3inf} = 1.2X_{3p}$; d, $X_{2inf} = 0.8X_{2p}$ and $X_{3inf} = 0.8X_{3p}$; e, $X_{2inf} = 0.7X_{2p}$ and $X_{3inf} = X_{3p}$.

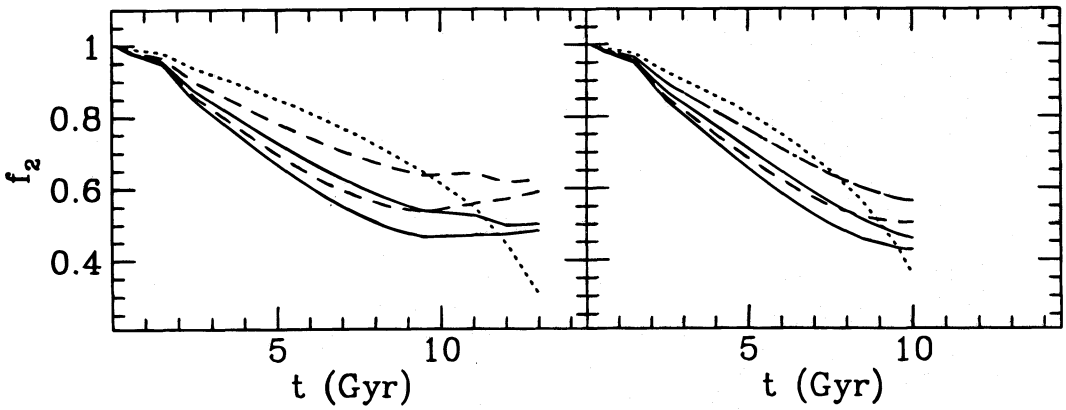

FIG. 5.—Deuterium survival factor f_2 as a function of time predicted by different models of the solar ring ($R = 8$ kpc). Models shown in the left panel assume 13 Gyr for the current age of the Galactic disk; those in the right panel assume 10 Gyr. In both panels, dotted curves correspond to no infall models, solid curves to models 1 (*upper curve*) and 25 (*lower curve*) with $X_{2\mathrm{inf}} = 0.8X_{2P}$, dashed curves to models 1 (*upper curve*) and 25 (*lower curve*) with $X_{2\mathrm{inf}} = X_{2P}$.

larger f_2 correlating with lower age. For models 1 and 25 the entire ranges are: $0.49 \leq f_{2\odot} \leq 0.73$; $0.43 \leq f_{20} \leq 0.62$; for the NI models: $0.70 \leq f_{2\odot} \leq 0.78$; $0.30 \leq f_{20} \leq 0.36$. Thus, for our range of models D astration is modest, typically by a factor of 1.3–2.0 at $t_\odot$ and a factor of 1.6–3.3 at t_0. Our models 1 and 25 have very little evolution in f_2 from $t_\odot$ to t_0 ($0.9 \leq f_{20}/f_{2\odot} \leq 1.2$ for $t_0 = 13$ Gyr; $1.3 \leq f_{20}/f_{2\odot} \leq 1.5$ for $t_0 = 10$ Gyr). This is entirely consistent with the solar system and ISM data: $X_{20}/X_{2\odot} = 1.6 \pm 0.6$ (e.g., Steigman & Tosi 1995).

In Figure 6 we show the time evolution of X_2 in the solar ring for models 1, 25, and NI for $t_0 = 13$ or 10 Gyr. Also shown in Figure 6 are the 2 σ ranges of the solar system (Geiss 1993; Steigman & Tosi 1995) and ISM (Linsky et al. 1992; Steigman & Tosi 1995) D abundances. For models 1 and 25 the ISM constraint dominates, limiting primordial D to $X_{2P} \leq 6 \times 10^{-5}$ (for $Y_P \lesssim 0.25$, $y_{2P} \lesssim 4 \times 10^{-5}$). Even for the NI model we find a restrictive bound $X_{2P} \leq 9 \times 10^{-5}$ ($y_{2P} \lesssim 6 \times 10^{-5}$).

In Figure 7 is shown the predicted radial distribution of D/H at present. The positive gradient is a natural consequence of larger D destruction in regions with larger SFR. The "data" are from Wannier (1980) but have been divided by a factor of 100 to facilitate comparison. While they

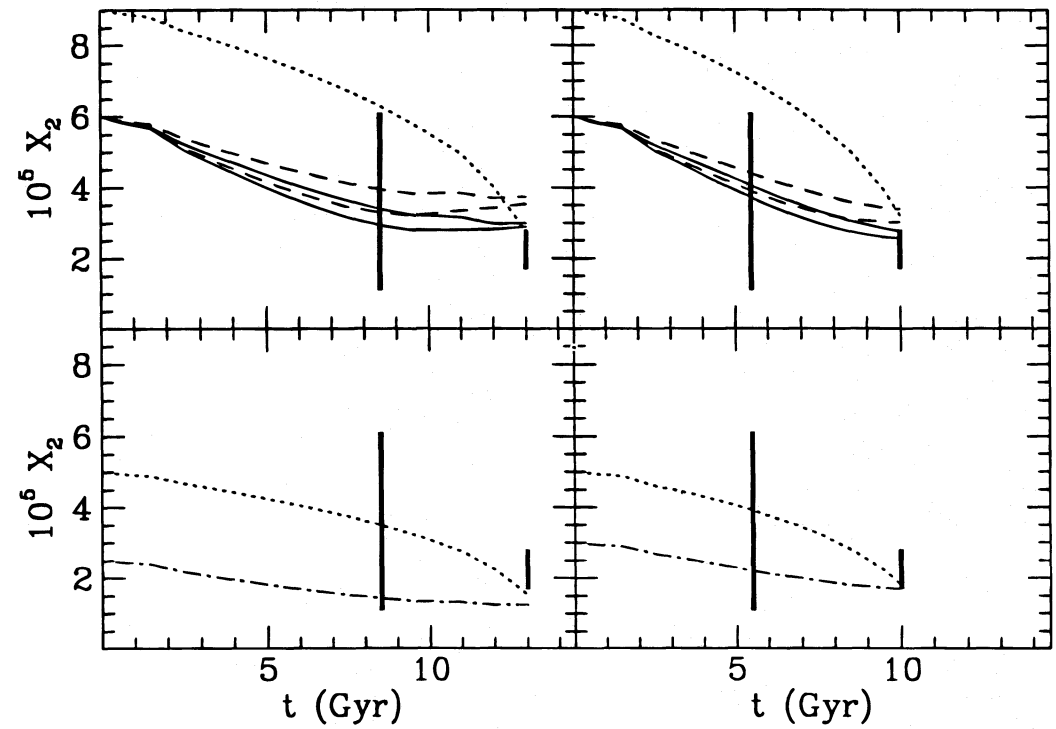

FIG. 6.—Evolution in the solar ring of the D abundance. Vertical bars give the 2 σ range for the abundances derived from solar system and local ISM observations (see text). Left panels correspond to a disk age of 13 Gyr, right panels to 10 Gyr. Models in the top panels assume the maximum value of primordial D consistent with the data; models in the bottom panels the corresponding minimum value. Dash-dotted lines correspond to "standard" models with primordial infall (1-B-Ia and 1_{10}-B-Ia), the other symbols are as in Fig. 5

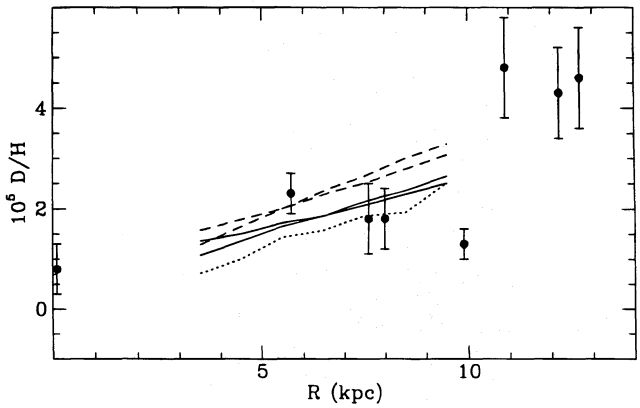

FIG. 7.—Current radial distribution of the D abundance resulting from the same models as Fig. 5 (same symbols as in that Figure). In each pair of curves of the same line-type, the steeper one corresponds to model 1 and the flatter one to model 25. Data points are from Wannier (1980) but arbitrarily divided by 100.

appear to reflect the expected radial distribution, they are some 2 orders of magnitude too large, possibly due to the chemical fractionation of deuterated molecules.

With the adoption of a chemical evolution model (e.g., 1. 25, or NI; $t_0 = 13$ or 10 Gyr; $X_{2\mathrm{inf}}/X_{2P} = 1.0$ or 0.8) the evolution of deuterium (with time and location in the Galaxy) is completely determined. Comparison with solar system and ISM observations then fixes (bounds) the primordial D abundance. For our "normal" models (not the NI models) we find $2.7 \leq 10^5 X_{2P} \leq 6.6$ (for $X_P \gtrsim 0.75$, $1.8 \lesssim 10^5 y_{2P} \lesssim 4.4$) which, for standard big bang nucleosynthesis (Walker et al. 1991; Thomas et al. 1996) bounds the nucleon-to-photon ratio η:$4.1 \lesssim \eta_{10} \lesssim 7.1$ ($\eta_{10} = 10^{10}\eta = 10^{10} n_N/n_\gamma$). Our (artificial) NI models prefer somewhat higher promordial D: $4.7 \leq 10^5 X_{2P} \leq 8.8$ ($3.2 \lesssim 10^5 y_{2P} \lesssim 5.9$; $3.5 \lesssim \eta_{10} \lesssim 5.1$).The modest astration we find is similar to many previous results (Audouze & Tinsley 1974; ST92; Galli et al. 1995; Fields 1995). Nonetheless, it may be possible to construct chemical evolution models with more destruction of D although consistency with all the observational constraints is quite improbable (Vangioni-Flam & Audouze 1988; Vangioni-Flam et al. 1994; Olive et al. 1995). An important test of all models is the evolution of ^{3}He (RST).

4. GALACTIC EVOLUTION OF ^{3}He: STANDARD MODELS

The evolution of ^{3}He is much more complex than that of D since ^{3}He may be destroyed, preserved and produced in differing proportions in stars of differing masses. Here, we have used the stellar results described in § 2 in concert with the large number of models summarized in Table 1. The key difference with our earlier work (ST92), which utilized similar models, is our allowance here for the production of new ^{3}He synthesized in lower mass stars. Following the results of § 2 in running the models, at each time step the adopted stellar yields are those corresponding to the X_{3f} of the dying stars. As anticipated by RST, the effect of ^{3}He production is large, dominating the evolution of ^{3}He.

In Figure 8 the evolution of ^{3}He is shown for a wide variety of choices of X_{2P}, X_{3P}, $X_{2\mathrm{inf}}$, $X_{3\mathrm{inf}}$ for model 1 and a present age of 13 Gyr. The vertical bar at 8.5 Gyr corresponds to the 2 σ range of abundances derived in the solar

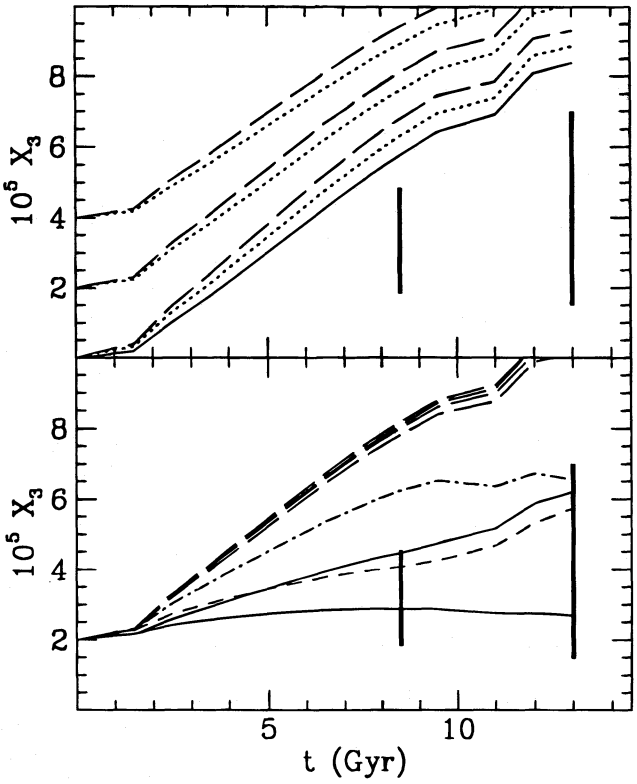

FIG. 8.—Evolution of the ^{3}He abundance in the solar ring as predicted by models 1. Vertical bars show the 2 σ range for the solar system and ISM abundances (see text for details). In the top panel all models adopt the standard stellar yields (see § 2 and Table 1) and assume primordial infall. They are in order of decreasing ^{3}He and D abundances (*i.e., from top to bottom*): 1-R-Ia, 1-J-Ia, 1-W-Ia, 1-I-Ia, 1-X-Ia, 1-H-Ia, 1-M-Ia. Models in the lower panel all start with the same primordial abundances of D and ^{3}He but have different adopted stellar yields and infall metallicity. From top to bottom they are: 1-W-(Ic, Ia, Ib, Id, Vb, VIIIb, IIIb, VIb).

system (Geiss 1993). Given the lack of ^{3}He determinations for the local ISM, the vertical bar at 13 Gyr corresponds to the 2 σ range of abundances derived by RBWB95 for H II regions between 6.4 and 10.3 kpc from the galactic center (but excluding W3 which definitely lies outside the average distribution and is the worst case for pressure broadening corrections). In the upper panel of Figure 8, the problem of excessive ^{3}He production identified by RST is clear. Using the stellar yields from § 2, it may be seen that there are no choices of X_{2P} and X_{3P} consistent with the range of ^{3}He abundances inferred from the solar system and/or ISM data. After the first few Gyr of evolution the contribution from newly synthesized ^{3}He overwhelms any primordial D + ^{3}He, and, even when $X_{2P} = X_{3P} = 0$, the ^{3}He abundances after 8.5 (13) Gyr are in excess of the solar system and ISM upper bounds.

The trends displayed in the upper panel of Figure 8 are easy to understand. For fixed choices of X_{3P}, $X_3(t)$ increases with increasing X_{2P} since any prestellar D is burned to ^{3}He, enhancing the main-sequence abundance of ^{3}He. Models which begin with higher X_{3P} always have higher ^{3}He abundances although, with time, the differences are reduced by the emerging dominance of the newly synthesized ^{3}He.

The upper four curves in the bottom panel of Figure 8 demonstrate the effect of the different choices for the infall abundances. However, these differences are small compared to the overall enhancement by stellar produced ^{3}He. As in

the upper panel, even in the absence of any primordial D or ^{3}He, the predicted ^{3}He abundances at the time or formation of the solar system and/or at present are in excess of the observational upper bounds.

Thus, our results confirm, with a vengeance, the problem identified by RST of ^{3}He overproduction when the contribution of new ^{3}He from low-mass stars is included in models of galactic chemical evolution (see also Galli et al. 1995). This conclusion is not modified when we used model 25, the NI model, or any of these models with a 10 Gyr disk age. We have, therefore, considered how we might have to modify the contribution of new ^{3}He from the low-mass stars in order to reconcile ^{3}He evolution with the observational data.

5. THE GALACTIC EVOLUTION OF ^{3}He: NONSTANDARD MODELS

As outlined in Table 1, in addition to our standard models (with the yields from § 2), we have considered several nonstandard models by modifying the ^{3}He yields from low-mass stars. As may be seen from the bottom panel of Figure 8 and in both panels of Figure 9, there are a variety of possible solutions to the problem of ^{3}He overproduction. The rapid increase in ^{3}He is most curtailed in models VI which follow the suggestion of Hogan (1995) that in stars less than 2.5 $M_\odot$, ^{3}He is destroyed on the giant branch before it can be returned to the ISM and the final envelopes of these stars therefore only contain an abundance X_{3f} corresponding to the equilibrium value ^{3}He/H $= 1 \times 10^{-5}$. However, Hogan's (1995) suggestion is in conflict with the normal ^{12}C/^{13}C ratios observed in stars more massive that 1.3–1.5 $M_\odot$ (Pinsonneault, 1995 private communication), as well as the observations of lithium (more fragile than ^{3}He) in some of them. Even worse, the observations of excess ^{3}He (X_3 of order 10^{-3}) in three planetary nebulae (Rood et al. 1992; RBWB95) appear to confirm that stars around 1.5 $M_\odot$ are efficient ^{3}He producers, in conflict with Hogan's proposal. Charbonnel (1995) has recently argued that the deep convective mixing responsible for the ^{3}He destruction in Hogan's suggestion takes place in stars experiencing the helium flash and gives an upper mass limit of 2 $M_\odot$ to the phenomenon. This would reconcile the deep-mixing ^{3}He destruction with the high PN abundances if the initial mass of the PN progenitor was at least 2 $M_\odot$. However, the three well-studied PNs have presumably originated from stars of initial mass 1.5 $M_\odot$ (Stanghellini 1995, private communication), thus lying in the range of stellar masses which should deplete and not enhance ^{3}He in the deep-mixing hypothesis.

To try to retain some of the benefit manifest in models VI, we have allowed ^{3}He to be reduced to its equilibrium value in lower mass stars (≤ 1 $M_\odot$ in models V, as suggested by Pinsonneault 1995, private communication; and ≤ 1.6 $M_\odot$ in models VII). However, since such low-mass stars have long lifetimes, the reduction in ^{3}He is only effective during recent epochs; solar system ^{3}He is still overproduced in both cases V and VII (see bottom panel of Fig. 8 where the two curves are so close that only one is shown). Even assuming a total ^{3}He destruction in stars below 1 $M_\odot$ (i.e., $X_{3f} = 0$, case IV) does not solve this inconsistency, since it provides results indistinguishable from case V.

Any other case, with upper mass cutoff for Hogan's ^{3}He destruction intermediate between 1 and 2.5 would either be inconsistent with the large abundance observed in PNs (if the cutoff is larger than 1.6 $M_\odot$) or inconsistent with the "low" solar system abundances (if it is smaller than 2 $M_\odot$). We have therefore tested some models assuming that ^{3}He is reduced to its equilibrium value in stars with mass between an arbitrary lower cutoff and 2.5 $M_\odot$. If the lower mass cutoff is around 1.3 $M_\odot$ (case VIII), smaller mass stars still produce large ^{3}He consistent with that observed in PNs and the ISM abundances predicted at the various epochs are consistent with the corresponding observed vaues (see Figs. 8 and 9).

In the models labelled II and III we have (arbitrarily) ignored new ^{3}He production and set $g_3 = 1$ for M below 2 $M_\odot$ (case II) or, between 1 and 2 $M_\odot$ (case III; see, e.g., Wasserburg, Boothroyd, & Sackmann 1995). As may be seen in Figure 8, models III are consistent with solar system and ISM data provided that the primordial abundances of D and/or ^{3}He are not too large.

Although some of the nonstandard models II–VIII may avoid overproduction of presolar and/or ISM ^{3}He the spatial distribution of ^{3}He observed in galactic H II regions (Bania et al. 1987; Rood et al. 1992; Balser et al. 1994; RBWB95) provides an important constraint on all such

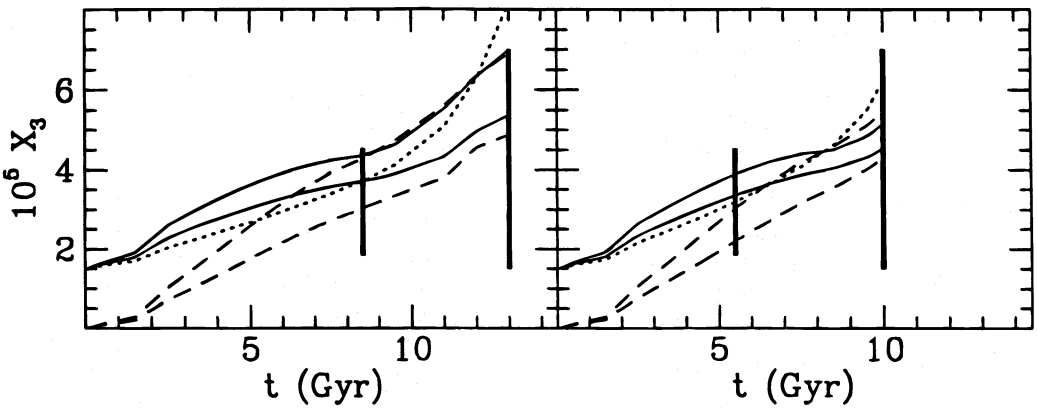

FIG. 9.—Evolution of the ^{3}He abundance in the solar ring as predicted by different chemical evolution models (1, 25, NI) using the same stellar yields and infall metallicity. The left-hand panel corresponds to a disk age of 13 Gyr and the right-hand panel to 10 Gyr. The lower and upper solid lines are models 1-T-IIIb and 25-T-IIb respectively (see Table 1); the lower and upper dashed lines are models 1-H-VIIIb and 25-H-VIIb; the dotted line is for NI-Z-III.

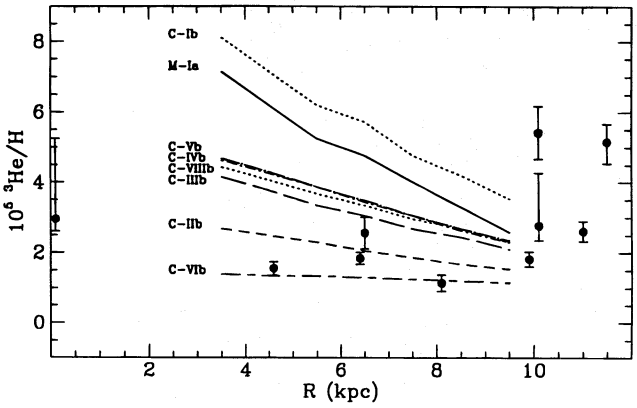

FIG. 10.—Predicted current radial distribution of the ^{3}He/H number ratio. Data points and error bars are from the H II region analysis by RBWB95 and the specific models are labelled.

models. The data are puzzling (see, e.g., Olive et al. 1995), exhibiting no very well defined trend of ^{3}He/H with galactocentric distance R (see Fig. 10). Indeed, in contrast to the theoretical expectation that ^{3}He/H should decrease with R (where the SFR is highest—in the inner galaxy—^{3}He/H should also be highest), the data hint at the opposite trend (see Fig. 10) typical of elements like H and D which are destroyed and not produced by stellar nucleosythesis. The only models which avoid a decreasing ^{3}He versus R relation are those with case VI yields, but cases II and, perhaps, III and VIII may also be consistent with the observed radial distribution, once all the uncertainties are taken into account.

We note that, despite the apparent conflicts of Hogan's (1995) suggestion with the ^{12}C/^{13}C, lithium and planetary nebulae data, comparison between case VI and the observational data still leads to a significant upper bound to primordial ^{3}He. For case VI we find that $X_{3\odot}/X_{3P} = 1.4$ so that for $X_{3\odot} \leq 4.5 \times 10^{-5}$ (Geiss 1993; Steigman & Tosi 1995), $X_{3P} \leq 3.2 \times 10^{-5}$ ($y_{3P} \leq 1.4 \times 10^{-5}$).

6. DISCUSSION

The evolution of deuterium depends solely on the chemical evolution model, and the D survival fraction, $f_2(t)$, is independent of the primordial abundance and of any stellar uncertainties since D is fully destroyed during the pre–main-sequence evolution. For our "best" models (1 and 25; Tosi 1988a, b), D is destroyed by only a modest factor (1.4–2.0) by the time of formation of the solar system and, by a slightly larger factor (1.6–2.4) up to the present epoch. Although the artificial NI models permit somewhat more destruction (by a factor of 2.8–3.3) by the present epoch, they actually destroy less D (1.3–1.4) up to the time of the formation of the solar system. The solar system and ISM data (Geiss 1993; Linsky et al. 1992) may be used along with models 1 and 25 (for a present age of either 10 or 13 Gyr) to bound (at the 95% CL) the primordial D abundance: $2.7 \leq 10^5 X_{2P} \leq 6.6$ ($1.8 \leq 10^5 y_{2P} \leq 4.4$). Comparing to the predictions of big bang nucleosynthesis (BBN) (e.g., WSSOK) permits us to bound the universal ratio of nucleons to photons: $4.1 \leq \eta_{10} \leq 7.1$. For our more extreme NI models we find: $4.7 \leq 10^5 X_{2P} \leq 8.8$ ($3.2 \leq 10^5 y_{2P} \leq 5.9$) and $3.5 \leq \eta_{10} \leq 5.1$.

In contrast to D, the evolution of ^{3}He is much more sensitive to the details of the chemical evolution model and, especially to the physics of stellar structure and evolution. A key component in our analysis here has been the computation of a new and extensive grid of stellar models covering a wide range of masses ($0.65 \leq M/M_\odot \leq 100$), heavy element abundances ($0.01 \leq Z/Z_\odot \leq 1$) and initial (main sequence) ^{3}He abundances ($10^{-5} \leq X_{3,\mathrm{MS}} \leq 10^{-3}$). We have then followed the ^{3}He evolution for models 1, 25, and NI with several choices for the present age of the disk (10 or 13 Gyr) and for the chemical composition of the infalling gas ($0.7 \leq X_{2\mathrm{inf}}/X_{2P} \leq 1.0$; $0.8 \leq X_{3\mathrm{inf}}/X_{3P} \leq 1.2$). As anticipated by RST, after the first few Gyr of evolution, stellar production of ^{3}He dominates (see, e.g., Fig. 8). This contribution from newly synthesized ^{3}He quickly overwhelms the primordial contribution and, even in the absence of any promordial ^{3}He (and D), we predict solar system and ISM ^{3}He abundances in excess of those inferred from the observational data (see also Galli et al. 1995, Tosi et al. 1994). Clearly, there is a problem and, until this conflict is resolved, ^{3}He cannot serve as a probe of BBN (RST). The problem may lie with the observational data and/or its interpretation. Or it could be that our models, or some of the ingredients therein, are the culprits.

The solar system ^{3}He data (meteorites, lunar soil and rocks, solar wind) have recently been reanalyzed by Geiss (1993). Although the size of the error estimates has increased compared, e.g., to those used in ST92, the central values remain unchanged. Consistency with our model predictions would require that the presolar ^{3}He abundance has been underestimated by more than a factor of 1.5–2.0.

The ISM data are more problematic. If, indeed, stellar production of new ^{3}He is occurring as indicated by the planetary nebulae observations (Rood et al. 1992; RBWB95), then X_3 should be higher where there is more stellar processing, in the inner galaxy. As may be seen in Figure 10, there is no observational evidence for such a trend. Indeed, the highest ^{3}He abundances are derived from data for the H II regions in the outer galaxy. The possibility that the ^{3}He abundances inferred from H II region radio observations are not reliable indicators of the current ISM values has also been invoked. Olive et al. (1995) have shown that unresolved structures in the nebulae may lead to an underestimate of their actual ^{3}He content but, only by a few tenths. On the other hand, the occurrence of a strong, ^{3}He depleted, Wolf-Rayet wind can reduce the ^{3}He abundance inside the H II region, although we presume that the external layers of many H II regions should still be uncontaminated and that a negative internal gradient should appear in the abundances derived from central to outer parts within the nebulae observed with sufficient spatial resolution. Besides, if an H II region exhibits depleted ^{3}He because of the pollution from the central Wolf-Rayet star, it should also show enhanced ^{4}He, which does not seem to be the case for the RBWB95 sample. Olive et al. (1995) have tried to understand the ^{3}He distribution as a reflection of the mass of the H II regions (more destruction of ^{3}He in the more massive H II regions). This radical explanation makes little sense to us (and, to them as well) since it would require that H II regions are more efficient processors of interstellar material than the Galaxy as a whole (since more than half the gas in these H II regions would have had to be cycled through the massive stars of the individual regions). Since the H II region data are hard to acquire and difficult to

analyze (see, e.g., RBWB95), work on both fronts is important, but beyond the scope of our analysis here. Very recently, Gloeckler & Geiss (1996) have measured for the first time the ^{3}He abundance in very local interstellar clouds. Their value, $^3\mathrm{He/H} = 2.2^{+0.9}_{-0.8} \times 10^{-5}$, is entirely consistent with the H II region results. So, here we have adopted the extant data, assumed that the inferred abundances are correct and investigated the implications for our models.

As may be seen in the Figures 8 and 9, the contribution from newly synthesized ^{3}He is large compared to the differences among the various model assumptions regarding the age of the disk, the infall abundances, the primordial abundances, and the specific models (1, 25, NI). Therefore, the prime suspect must be our estimates of the ^{3}He yields from low- and intermediate-mass stars (Rood 1972; Galli et al. 1994; Hogan 1995; Wasserburg et al. 1995). To explore this avenue we have considered a series of nonstandard alternatives to our standard models. Indeed, several suggestions have been published for physical mechanisms to suppress the overproduction of stellar ^{3}He. They are related to low-energy resonances or to deep convective mixing (e.g., Galli et al. 1994; Hogan 1995; Wasserburg et al. 1995), but none of them seems fully consistent with all the available data. In our cases II, III, VI, and VIII the suppression of stellar-produced ^{3}He may be sufficient to flatten the X_3 versus t relation enough so that consistency with the local data may be found provided that the primordial abundances are small enough. However, it must be emphasized that if the detections of excess ^{3}He in planetary nebulae reported by Rood et al. (1992) and RBWB95 are confirmed, some of these alternatives (II and VI) are excluded. By comparing the model predictions with all the available constraints, we find that only case III is sufficiently compatible with all the data, despite its shallow negative gradient in the X_3 versus R relation. In this case we may use the solar system data to bound the primordial abundance of ^{3}He from above and, the nucleon-to-photon ratio from below.

7. CONCLUSIONS

We have tracked the evolution of the abundances of D and ^{3}He in a variety of chemical evolution models which incorporate the results of a newly computed grid of stellar structure and evolution models. We have confirmed that D is fully destroyed during the pre–main-sequence evolution and, therefore, its galactic evolution is simple. For the range of our models (see § 3) we find only modest destruction of D and, using the solar system and ISM data in concert with our "best" models, we bound the primordial (pre-galactic disk) abundance,

$$2.7 \leq 10^5 X_{2P} \leq 6.6\ , \quad 1.8 \leq 10^5 y_{2P} \leq 4.4\ . \tag{1}$$

For consistency with the predictions of standard BBN (WSSOK), we require that the universal ratio of nucleons (baryons) to photons lie in the range,

$$4.1 \leq \eta_{10} \leq 7.1\ . \tag{2}$$

In terms of the baryon density parameter, Ω_B, ($\Omega_B h_{50}^2 = 0.015\eta_{10}$; $H_0 = 50 h_{50}$ km s^{-1} Mpc^{-1}),

$$0.06 \leq \Omega_B h_{50}^2 \leq 0.10\ . \tag{3}$$

For our NI models the X_{2P} estimate is somewhat higher and the bounds on the baryon density slightly lower.

Our stellar models, which account for the evolution of ^{3}He (destruction, survival, production) reveal that for low-mass stars the production of newly synthesized ^{3}He is very important for the evolution of Galactic ^{3}He. Indeed, for all of our standard models (§ 4) production of new ^{3}He is so dominant that even in the absence of any pregalactic D and/or ^{3}He, ^{3}He is overproduced compared to the solar system and ISM data. Until this conflict is resolved it is difficult to see how ^{3}He can be used as a probe of BBN (RST). Setting aside the possibility that the problem lies with the observational data, we have explored a series of nonstandard models (§ 5) in which some or all of the newly synthesized ^{3}He is assumed to be destroyed before being returned to the ISM. We find that if this suppression of ^{3}He occurs only in stars $\leq 1\ M_\odot$, the depletion is "too little, too late" to resolve the discrepancy with the solar system data. In contrast, ^{3}He destruction in stars with masses in the range 1–2 $M_\odot$ (Wasserburg et al. 1995) can reconcile our models with the data provided that the initial ^{3}He abundance is not too large. In this case we recover a lower bound to the baryon density which is consistent with that derived from the D evolution data (see eqs. [1–3]). It remains to be seen whether this "fix" will be permitted by the PNs and or ^{12}C/^{13}C data.

M. T. warmly thanks Letizia Stanghellini, Daniele Galli, and Claudio Ritossa. G. S. thanks M. Pinsonneault for valuable and simulating discussions. We are also pleased to thank the referee, F. Palla. The work of G. S. is supported at Ohio State by the Department of Energy (DE-AC02-76-ER01545); part of this work was done while G. S. was a visitor at the Instituto Astronomico e Geofisico (Sao Paulo, Brazil) and he thanks them for hospitality and assistance.

REFERENCES

Audouze, J., & Tinsley, B. M. 1974, ApJ, 192, 487
Bahcall, J. N., & Ulrich, R. K. 1988, Rev. Mod. Phys., 60, 297
Balser, D. S., Bania, T. M., Brockway, C. J., Rood, R. T., & Wilson T. L. 1994, ApJ, 430, 667
Bania, T. M., Rood, R. T., & Wilson, T. L. 1987, ApJ, 323, 30
Black, D. C. 1971, Nature Phys. Sci., 234, 148
———. 1972, Geochim. Cosmochim. Acta, 36, 347
Bolte, M. 1994, ApJ, 431, 223
Carswell, R. F., Rauch, M., Weymann, R. J., Cooke, A. J., & Webb, J. K. 1994, MNRAS, 268, L1
Charbonnel, C. 1995, preprint
Dearborn, D. S. P. 1992, Phys. Rep., 210, 367
Dearborn, D. S. P., & Eggleton, P. P. 1976, QJRAS, 17, 448
Dearborn, D. S. P., Griest, K., & Raffelt, G. 1991, ApJ, 368, 626
Dearborn, D. S. P., Schramm, D. N., & Steigman, G. 1986, ApJ, 203, 35 (DSS)
Edmunds, M. G. 1994, MNRAS, 270, L37
Eggleton, P. P. 1967, MNRAS, 137, 243
———. 1968, MNRAS, 143, 87
Fields, B. D. 1995, ApJ, in press
Galli, D., Palla, F., Ferrini, F., & Penco, U. 1995, ApJ, 443, 536
Galli, D., Palla, F., Straniero, O., & Ferrini, F. 1994, A0J, 432, L101
Geiss, J. 1993 in Origin and Evolution of the Elements, ed. N. Prantzos, E. Vangioni-Flam, & M. Cassé (CUP, U.K.), 89
Geiss, J., & Reeves, H. 1972, A&A, 18, 126
Giovagnoli, A., & Tosi, M. 1995, MNRAS, 273, 499
Gloecker, G., & Geiss, J. 1996, Nature, submitted
Hogan, C. J. 1995, ApJ, 441, L17
Huebner, W. F., Merts, A. L., Magee, N. H., Jr., & Argo, M. F. 1977, Astrophysical Opacity Library (LASL, LA-6760-M)
Iben, I. Jr. 1967, ApJ, 147, 624
Iglesias, C. A., & Rogers, F. J. 1990, ApJ, 360, 221
———. 1992, ApJ, 397, 717
Linsky, J. L., et al. 1992, ApJ, 402, 694

Matteucci, F., & François, P. 1989, MNRAS, 239, 885
Olive, K. A., Rood, R. T., Schramm, D. N., Truran, J., & Vangioni-Flam, E. 1995, ApJ, 444, 680
Olive, K. A., & Steigman, G. 1995, ApJS, 97, 49
Pagel, B. E. J., Simonson, E. A., Terlevich, R. J., & Edmunds, M. G. 1992, MNRAS, 255, 325
Pinsonneault, M. 1995, private communication
Prantzos, N. 1995, A&A, in press
Rood, R. T. 1972, ApJ, 177, 681
Rood, R. T., Bania, T. M., & Wilson, T. L. 1992, Nature, 355, 618
Rood, R. T., Bania, T. M., Wilson, T. L., & Balser, D. N. 1995, in The Light Element Abundances, ed. P. Crane (Berlin: Springer) 201 (RBWB95)
Rood, R. T., Steigman, G., & Tinsley, B. M. 1976, ApJ, 207, L57 (RST)
Skillman, E. D., Terlevich, R. J., Kennicutt, R. C., Garnett, D. R., & Terlevich, E. 1994, ApJ, 431, 172
Songaila, A., Cowie, L. L., Hogan, C. J., & Rugers, M. 1994, Nature, 368, 599
Spite, F., & Spite, M. 1982, A&A, 115, 357
Steigman, G. 1994, MNRAS, 269, P53
Steigman, G., & Tosi, M., 1992, ApJ, 401, 150 (ST92)
Steigman, G., & Tosi, M. 1995, ApJ, 453, 173
Thomas, D., Hata, N., Scherrer, R., Steigman, G., & Walker, T. 1996, in preparation
Thorburn, J. 1994, ApJ, 421, 318
Tinsley, B. M. 1980, Fundam. Cosmic Phys., 5, 287
Tosi, M. 1988a, A&A, 197, 33
———. 1988b, A&A, 197, 47
Tosi, M., Steigman, G., & Dearborn, D.S.P. 1994, in The Light Element Abundances, ed. P. Crane (Berlin: Springer) 228
Tyler, D. 1995 in QSO Absorption Lines, ed. G. Meylan (Berlin: Springer), in press
Vagioni-Flam, E., & Audouze, J. 1988, A&A, 1993, 81
Vagioni-Flam, E., Olive, K. A., & Prantzos, N. 1994, ApJ, 427, 618
Vassiliadis, E., & Wood, P. R. 1993, ApJ, 413, 641
Walker, T. P., Steigman, G., Schramm, D. N., Olive, K. A., & Kang, H. S. 1991, ApJ, 376, 51 (WSSOK)
Wannier, P. G. 1980, ARA&A, 18, 366
Wasserburg, G., Boothroyd, A., & Sackmann, I.-J., 1995, ApJ, 447, L37
Yang, J., Turner, M. S., Steigman, G., Schramm, D. N., & Olive, K. A. 1984, ApJ, 281, 493 (YTSSO)